Raman scattering from electronic excitations in Ge†

J. Doehler*
Department of Physics and The James Franck Institute, University of Chicago, Chicago, Illinois 60637
(Received 30 September 1974; revised manuscript received 20 May 1975)

Polarized Raman spectra of pure, gallium-doped, and arsenic-doped germanium have been measured as a function of impurity concentration and temperature, using the output of a 2.1-μm laser to which germanium is transparent. The impurity concentration ranged from 6.3×10^{15} cm^{-3} (semiconducting regime) to 5.5×10^{17} cm^{-3} (metallic regime). The acceptor spectrum has been resolved into two lines whose polarization characteristics have been measured and deduced group theoretically. The donor spectrum consists, at low impurity concentration, of a single valley-orbit Raman line whose polarization selection rules have been found to be, in good agreement with group theory, identical to those of the zone-center optic phonon of the host crystal. The effects of wave-function overlap at higher impurity concentration on the electronic states have been systematically studied. In particular, the donor spectra have been studied as the crystal undergoes the Mott transition. Polarization studies of the light scattered from metallic samples show that intervalley fluctuations are responsible for the observed single-particle excitations.

I. INTRODUCTION

Raman scattering in semiconductors has been a fruitful area of investigation in recent years. It has yielded a wealth of information on the band structures, on the impurity states, on the dynamics of electrons or holes in the conduction and/or valence bands, and on the interaction of these electrons or holes with elementary excitations. In contrast, only phonon processes have been observed in the many Raman experiments which have been performed on germanium in the past several years.[1-4] At low temperature ($T\lesssim20$ K), germanium has a band gap of 0.74 eV[5], and strongly absorbs the visible exciting light used in experiments performed to date; the penetration depth of visible light in germanium is of the order of 1000 Å. In particular, the strong absorption has precluded the observation of electronic Raman processes associated with donor and acceptor impurity states. It is in order to observe these electronic Raman processes, including acceptor and donor Raman transitions and single-particle excitations from holes and electrons, that a 2.098-μm (0.59-eV) Raman laser source has been built and employed in the study of pure, gallium-doped, and arsenic-doped germanium.

Not only have the Raman spectra of Ge(As) been measured in the usual way, i.e., with low-impurity-concentration samples, in order to test the applicable existing theories of light scattering in semiconductors, but the spectra have also been systematically studied for the first time as a function of impurity concentration. This systematic study brings insight into the electron-electron interaction, which, at high impurity concentration, leads to the Mott transition. Doped germanium, a material which is usually regarded as being the ideal testing ground for the Mott transition, is a unique system in which the Mott transition occurs at a relatively low impurity concentration. Consequently, the samples examined in this study remain practically transparent to near-infrared radiation, even in the metallic regime.

This paper, in which we present the complete details of the study of electronic processes, including the Mott transition, is organized as follows: Section I will give a brief review of the work on semiconductors which has bearing on this paper. Section II will describe the Raman spectrometer used in this study. The experimental results and their discussions will be presented in Sec. III. Section IV will present our conclusions. Preliminary discussions of some of the results reported here have appeared elsewhere.[6,7]

Raman scattering from transitions between electronic levels of an impurity in a crystal was first proposed by Elliott and Loudon.[8] This electronic Raman effect was observed for the first time by Hougen and Singh who studied rare-earth crystals.[9] The first observation of Raman scattering from impurity levels in semiconductors was made by Henry *et al.* on gallium phosphide containing Zn and Mg acceptors,[10] while Raman transitions between donor and acceptor levels in a semiconductor were first observed by Wright and Mooradian in doped silicon.[11,12] Wright and Mooradian also observed transitions between acceptor levels in silicon and in gallium arsenide, and from donor levels in aluminum antimonide.[11-13] Cherlow *et al.*[14] verified the assignment of the valley-orbit transition by repeating the experiment of Wright and Mooradian[11] with the simultaneous application of uniaxial stress and a magnetic field. Valley-orbit Raman transitions were also seen in gallium phosphide[15] and in silicon carbide,[16-18] which exhibits interesting effects owing to the different inequivalent impurity sites. The first observation of donor transitions involving states outside of the valley-orbit-split manifold was

made on cadmium sulphide doped with chlorine,[19] a material which does not exhibit a valley-orbit splitting.

Information about the spectrum of collective modes and single-particle excitations can also be obtained from the Raman spectra. Light-scattering experiments on solid-state plasmas have been the subject of considerable theoretical and practical interest in recent years; they have led, for instance, to the invention of the spin-flip Raman laser. Experiments performed in a magnetic field will not be discussed here. Collective plasma modes (plasmons) can be observed when their energies are larger than the binding energy of the carriers involved. Collective modes, however, have been observed only in polar crystals lacking inversion symmetry and in which the plasmon can couple to the LO phonon giving rise to mixed modes.[16,20-27]

Single-particle excitations, in which charged carriers are scattered out of the Fermi sea and in which the frequency shift is proportional to the carrier velocity, have been extensively studied.[23,24,28-32] The Raman spectrum is a direct measure of the velocity distribution of the charge carriers and the polarization characteristics of the Raman photons yield information on the coupling mechanism responsible for the scattering. An excellent review of single-particle excitations can be found in Ref. 33.

The phenomenon now know as the Mott transition was first observed by Busch and Labhart[34] in conductivity experiments. It was found that the resistivity of silicon carbide showed a large drop as the impurity concentration was increased to a critical value n_c. Measurements on phosphorous-doped silicon,[35] germanium,[36,37] silicon carbide,[38] indium antimonide,[39] lead sulphide,[40] and gallium arsenide[41] showed that the metallic transition was a general phenomenon in doped semiconductors. From Hall-coefficient measurements,[35-37] it is known that the number of free carriers in a doped semiconductor increases sharply as the concentration approaches n_c; above n_c, the number of free carriers is just equal to the number of impurities. The critical concentration n_c depends upon the host material and, in general, upon the impurity. The increase in nuclear-spin–lattice relaxation time T_1 with concentration near n_c,[42] and the temperature dependence of T_1 above n_c, are consistent with such an explanation. ESR experiments[43,44] show that even below n_c a large fraction of the electrons are moving over clusters of donor sites instead of each being bound to an individual donor. While all the above-mentioned experiments show a threshold for carrier delocalization, they do not give any clues as to the mechanisms responsible for the Mott transition. The negative magnetoresistance found in doped semiconductors near n_c[39-41] seems to indicate that a substantial fraction of the electrons remain localized above n_c (Anderson localization).[45] Many features of the magnetoresistance however remain unexplained; in particular, the nondisappearance of the negative magnetoresistance at higher concentrations. NMR measurements[46] also seem to indicate the presence of localized electrons above n_c. This is in agreement with the Raman scattering measurements of Colwell and Klein[16] on degenerate silicon carbide, in which some semiconducting character (i.e., bound electrons) is observed above n_c.

Systematic Raman or infrared absorption studies of the Mott transition have so far been precluded by the high absorption coefficient found in most materials at an impurity concentration near n_c. Pankove and Aigrin[47] measured the wavelength dependence of the absorption coefficient of arsenic-doped germanium. It shows a sharp minimum near 2.1 μm. The exciting radiation of short wavelength (<0.6 μm) used in previous Raman experiments[1-4] is strongly absorbed by interband transitions. At long wavelength, the free-carrier absorption (or Drude process) dominates; also, detector efficiencies and phonon Raman cross sections (proportional to ω^4) decrease markedly with increasing wavelength. Therefore, the ideal spectral region in which to perform Raman experiments on arsenic-doped germanium lies near 2.1 μm, an intermediate wavelength at which the samples remain practically transparent.

II. EXPERIMENTAL PROCEDURE

The 2.1-μm Raman spectrometer used in the experiment is unique and differs from conventional Raman spectrometers by utilizing a 2.1-μm *ABC*-YAlG (yttrium aluminum garnet doped with various concentrations of Er, Tm, Ho, and Yb) laser and a PbS photodetector. The description of the Raman spectrometer in this section will therefore be given with particular emphasis on these two instruments.

A. 2.1-μm laser

The cooling system discussed in Ref. 48 has been modified to adapt a high-speed centrifugal liquid-nitrogen pump.[49] Also, carbon tetrachloride is circulated in the outer vacuum jacket in place of water to provide cooling; it was found that water absorbed a substantial part of the radiation from the exciting light which would otherwise have contributed to the optical pumping. It was also found that a vacuum of the order of 10^{-6} Torr was needed in the laser head for long runs. At higher pressures, the residual gases tend to condense on the laser rod which is at cryogenic temperatures; this condensation drastically effects the properties of

the antireflection coatings of the laser rod and reduces laser output. With the laser so modified, output powers in excess of 25 W cw at 2.1 μm were obtained.

Typical output powers used during the experiments reported here were 6 W. To obtain that power level only 950-W electrical input to the pump lamps was required. With this reduced input, the liquid-nitrogen consumption was reduced to 1.5 cm^3/sec.

B. PbS photodetector

A PbS photodetector element was used in the experiment reported here. It was purchased from and designed by Santa Barbara Research Center[50] to have its highest sensitivity at a temperature of 77 K. The element size was 3.5×0.5 mm^2.

A series of diaphragms forming a baffle designed to trap the room-temperature blackbody radiation were placed in front of the detector element. Each diaphragm consisted of a sheet of brass 0.1 mm thick and 12 mm in diameter; a hole was punched in its center, the dimensions of which were determined by mapping the rectangular beam of light which emerged from the spectrometer exit slit and was focused onto the detector. A series of six such diaphragms were soldered into an assembly, the diaphragms being spaced 2 mm apart along the optical path. The assembly was painted matte black to absorb the parasitic rays, and mounted in front of the detector. The baffle was fitted with an optical filter (obtained from Optical Coating Laboratory, Inc.[51]) which had better than 75% average transmission between 1.973 and 2.464 μm. The light beam incident on the detector had an equivalent f number of 2. The baffle assembly as well as the optical filter and the detector were maintained at liquid-nitrogen temperature during the experiment. The temperature could be checked by measuring the detector resistance (6.9 MΩ at 77 K) and/or the output of a thermocouple placed on the cold filter. Prior to use, the detector, as well as the filter and diaphragm assembly was baked for 2 h at 80 °C in a vacuum and in darkness to neutralize the deleterious effects of overexposure to light to which the detector might have been subjected during its installation.

The sensitivity of the detector was measured at 2.1 μm by using the output of the *ABC*-YAlG laser. The laser output was spatially filtered by passing it through a pinhole. A divergent beam of known power density was therefore incident on the detector. This power density was reduced by placing a series of liquid absorption cells containing a mixture of carbon tetrachloride and methanol in front of the detector. The absorption coefficient of the cells at 2.1 μm could be adjusted over several orders of magnitude by carefully controlling the concentration ratio of methanol (which strongly absorbs at 2.1 μm) to carbon tetrachloride (which is transparent at 2.1 μm). The measured D^* of the detector at 2.1 μm was 2.4×10^{12} cm $Hz^{1/2}$/W.

Typical integration times used to record spectra were 10 sec, which is an improvement of a factor of 10 over the typical integration times reported in Ref. 6. The long intrinsic relaxation time of the detector ($\simeq$150 msec) necessitated a chopping frequency of the order of 5 Hz.

C. Other experimental equipment

The other experimental equipment used in the experiment was basically identical to that used in Ref. 6. The double monochromator[52] was equipped with 600 grove/mm gratings blazed at 1.3 μm with polarization characteristics at 2.1 μm such that the thruput of the instrument was about a factor of 10 lower for light polarized parallel than for light polarized perpendicular to the grating grooves. A Glan-Taylor[53] polarizer was used in front of the entrance slit of the monochromator when polarized spectra were being recorded.

The linearly polarized output of the laser was chopped at 5.5 Hz and focused in the sample with a quartz lens through the bottom window of the cryostat. The exciting light, after having traversed the sample, was deflected towards a side window with a small gold-plated copper mirror placed above the sample. The laser light was then absorbed in a power meter which was used to monitor the laser output. The scattered light was collected at 90°, through a Dewar side window. The over-all sensitivity of the Raman spectrometer was high enough to record the second-order spectrum of pure germanium.[54]

III. RESULTS AND DISCUSSIONS

A. Raman scattering by zone-center phonon

The Raman selection rules for the light scattered by the zone-center phonon in germanium have been studied before[1-4]; however, a number of electronic processes in germanium have been found to have the same Raman selection rules as the phonon. It is therefore useful to describe the selection rules here briefly.

Germanium has only one triply degenerate optic phonon at the zone center.[1-4] This phonon is Raman active, of symmetry T_{2g}, and its Raman tensors[55] with respect to the crystal cubic axes [100], [010], and [001] are given by[56]

$$\begin{pmatrix} 0 & a & 0 \\ a & 0 & 0 \\ 0 & 0 & 0 \end{pmatrix}, \quad \begin{pmatrix} 0 & 0 & a \\ 0 & 0 & 0 \\ a & 0 & 0 \end{pmatrix}, \quad \begin{pmatrix} 0 & 0 & 0 \\ 0 & 0 & a \\ 0 & a & 0 \end{pmatrix}. \tag{1}$$

Therefore, with the incident and scattered light both propagating along cubic axes, the light scat-

tered by the phonon is observable only in the crossed polarization configuration since only off-diagonal elements of the Raman tensors are nonzero. In the standard notation[57] $i(jk)l = \vec{k}_0(\vec{\lambda}_0\vec{\lambda}_1)\vec{k}_1$, the phonon is observable in the $Z(XY)X$ scattering geometry, but not in the $Z(YY)X$ scattering geometry; here X, Y, and Z are laboratory axes and $\vec{X} \parallel [100]$, $\vec{Y} \parallel [010]$, and $\vec{Z} \parallel [001]$. The standard notation has the advantage of emphasizing that we are probing the (jk) component of the Raman tensor. With the crystal orientation $\vec{X}' \parallel [110]$, $\vec{Y}' \parallel [\bar{1}10]$, and $\vec{Z}' \parallel [001]$, the Raman tensor T becomes

$$T' = RTR^{-1}, \tag{2}$$

where R is the rotation matrix which brings the axes [100], [010], and [001] into [110], $[\bar{1}10]$, and [001], respectively. The transformed Raman tensors can be straightforwardly calculated:

$$\begin{pmatrix} -a & 0 & 0 \\ 0 & a & 0 \\ 0 & 0 & 0 \end{pmatrix}, \quad \frac{\sqrt{2}}{2}\begin{pmatrix} 0 & 0 & a \\ 0 & 0 & a \\ a & a & 0 \end{pmatrix}, \quad \frac{\sqrt{2}}{2}\begin{pmatrix} 0 & 0 & -a \\ 0 & 0 & a \\ -a & a & 0 \end{pmatrix}. \tag{3}$$

Therefore, in the primed crystal orientation, the phonon in germanium should be observed in the $Z'(Y'Y')X'$ geometry, but not in the $Z'(X'Y')X'$ scattering geometry.

The polarization measurements reported in Ref. 6 are in excellent agreement with the Raman selection rules derived above.

B. Raman scattering from donor states

An excess electron introduced by a donor impurity such as arsenic binds to the impurity ion and forms discrete energy levels which are, in the effective-mass approximation,[58] hydrogenic. Because of the large dielectric constant of the host material and the low effective mass of the electrons near the conduction-band minima, the Bohr radius associated with the donor ground state is very large, of the order of 35 Å. But in an indirect gap material such as germanium, with its four equivalent conduction-band minima, the valley-orbit interaction[59,60] splits the fourfold degenerate ground state into a $1s(A_1)$ singlet and a $1s(T_2)$ triplet. Here, A_1 and T_2 are irreducible representations of the T_d point group associated with the site symmetry of the impurity atom. The qualitative effect of the valley-orbit interaction is to lower the energy of the ground state. Since the wave function of the $1s(A_1)$ state has a larger magnitude at the impurity site than the $1s(T_2)$ wavefunction, the singlet state is more affected than the triplet state, creating a "valley-orbit" splitting. The magnitude of that splitting has been calculated by a number of authors.[59,60] In germanium, it is about 4 meV.

Colwell and Klein[16] have calculated the Raman cross section for a process starting on the $1s(A_1)$ ground state and terminating on the $1s(T_2)$ excited state. They used the wave function for the $1s$ states given by Kohn[58]:

$$\Psi(\vec{r}) = \sum_{j=1}^{4} \alpha_j^{(\nu)} F_j(\vec{r}) u_j(\vec{r}) e^{i\vec{k}_j\cdot\vec{r}}, \tag{4}$$

where $F_j(\vec{r})$ is an envelope function which satisfies the "effective-mass equation"[58] and whose magnitude does not change significantly within one unit cell; $\alpha_j^{(\nu)}$ are numerical coefficients for the group representation (ν) of the impurity Hamiltonian; and $u_j(\vec{r})$ is the periodic part of the Block function at the jth minimum. Colwell and Klein used only the terms in $\vec{p}\cdot\vec{A}$ which appear in the electron-photon interaction Hamiltonian, and a two-band model in which the inverse effective-mass tensor $(m/m_{\alpha\beta})$ is given by $\vec{k}\cdot\vec{p}$ perturbation theory.[61] Their result is

$$\frac{d^2\sigma}{d\Omega_1\, d\omega_1} = \left(\frac{e}{mc^2}\right)^2 \left(\frac{\omega_1}{\omega_0}\right)\left(\frac{E_G^2}{E_G^2 - (\hbar\omega_0)^2}\right) \delta(\omega - \omega_{VO}) \left| \sum_{\alpha,\beta=1}^{3} (\vec{\lambda}_0)_\alpha (\vec{\lambda}_1^{\,*})_\beta \sum_{j=1}^{4} \alpha_j^{(\nu)} \alpha_j^{(\nu')} \left[\left(\frac{m}{m^*}\right)_{\alpha\beta} - \delta_{\alpha\beta}\right]_j \right|^2, \tag{5}$$

where ω_0 (ω_1) is the frequency of the incident (scattered) light, $\vec{\lambda}_0(\vec{\lambda}_1)$ the corresponding polarization vectors, ω_{VO} is the valley-orbit splitting, $\alpha_j^{(\nu)}$ are numerical coefficients for the group representation (ν) of the ground state, and $\alpha_j^{(\nu')}$ are numerical coefficients for the group representation (ν') of the particular state excited. To obtain Eq. (5), it was assumed that $\vec{p}$ does not operate on $F_j(\vec{r})$. The assumption that $\vec{p}$ does not operate on $F(\vec{r})$ implies that no Raman process incorporating transitions out of the $1s$ manifold is allowed. Klein[62] finds similar results using the terms in $\vec{A}^2$, which appear in the electron-photon interaction Hamiltonian. Also, Wright and Mooradian,[11] who used a three-band model, showed that Raman processes out of the $1s$ manifold would be weak and thus difficult to observe. Thus, for shallow donors in germanium, we expect a single Raman line originating from a transition within the valley-orbit-split ground state.

Figure 1 shows the Raman spectrum of Ge doped with 6.3×10^{15} cm^{-3} As impurities. The feature at

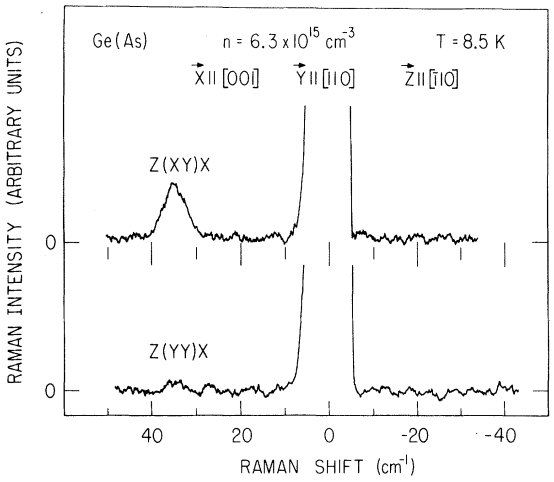

FIG. 1. Polarized Raman spectra of arsenic-doped germanium. Both spectra were recorded using the same system gain.

35 cm^{-1} does not appear in the pure material, and this feature grows in magnitude as the temperature is lowered. It is therefore due to transitions among donor levels. We believe it to be the valley-orbit Raman line for the following reasons:

(i) The energy of 35 ± 1 cm^{-1} is in good agreement with the value of 34.12 ± 0.16 cm^{-1} which has been deduced from infrared absorption measurements[63,64] for the valley-orbit splitting in Ge(As).

(ii) If the feature at 35 cm^{-1} arises from the $1s(A_1)$ to $1s(T_2)$ Raman transition, the components of its Raman tensors must transform according to the T_2 irreducible representation of the T_d point group. The three Raman tensors corresponding to ${}^{56}T_2$ have the same structure as the Raman tensors of the T_{2g} zone-center phonon [Eq. (1)]. Group theory thus predicts identical Raman selection rules for the phonon and the valley-orbit line. The spectra in Fig. 1 show that our polarization measurements are in very good agreement with the calculated Raman selection rules.

(iii) The measured ratio of valley-orbit to phonon scattering efficiency has been shown to be[6] in very good agreement with the ratio calculated using Eq. (5).

(iv) Finally, no other electronic Raman transition is observed, in good agreement with the calculations of Colwell and Klein[16] and of Wright and Mooradian.[11]

C. Raman scattering from acceptor states

Acceptor states differ from donor states in the following fashion: the bound states are localized above the valence-band maximum, instead of below the conduction-band minima. While germanium has only one valence-band maximum in the Brillouin zone, and hence no valley-orbit interaction, the acceptor spectra are more complex than the donor spectra because of the degeneracy of the valence band at the zone center. In addition, the spin-orbit interaction splits the sixfold degenerate valence band into a fourfold degenerate upper band and a twofold degenerate lower band. Thus, the spin-orbit interaction must be considered explicitly in the acceptor-states calculations. The acceptor-states calculations then consist of solving six coupled effective-mass equations.[58] A number of authors[62,65-70] have solved the set of coupled equations using the variational method. The disadvantage of the brute-force variational method is that it does not give any clear insight into the acceptor spectrum. In particular, the dependence of the spectra upon the energy-band parameters is lost. Consequently, other than a brief discussion by Wright and Mooradian[13] and by Klein,[62] there is no definitive analysis in the literature on the theory of light scattering by acceptor transitions. The spherical model of Baldereschi and Lipari[71] is too recent to have been applied to the theory of light scattering.

The spin-orbit interaction in germanium (0.29 eV) is large compared to the typical shallow-acceptor binding energy ($\simeq 0.01$ eV). We can therefore expect the acceptor states to be derived from the four Bloch states of the upper valence band, with little admixture of Bloch states from the lower band. The state associated with a given acceptor level must therefore form a basis for a Γ_6, Γ_7, or Γ_8 irreducible representation of the full double tetrahedral symmetry group of the impurity. (Here we adopt the group-theoretical notation more commonly used for electronic states.)

Figure 2 shows the Raman spectra of gallium-doped germanium recorded with several polarization configurations. The two features at 65 and 74 cm^{-1} shown in Fig. 2 do not appear in the pure material, and their magnitudes increase as the temperature is lowered. The two lines therefore originate from Raman transitions between acceptor levels. These Raman spectra can be compared with the infrared absorption spectra measured by Jones and Fisher.[72] The positions of the Raman lines at 65 and 74 cm^{-1} are in good agreement with the energies of 64.7 and 74.1 cm^{-1} measured for the "E" and "C" lines, respectively, by Jones and Fisher. The "E" line corresponds to a transition between the $1s$ ground state to the $2s$ excited state, while the "C" line corresponds to a transition between the $1s$ ground state to the $3f$ excited state. The "E" line is found to be weak in infrared absorption with respect to the "C" line, while the Raman spectrum shows that the two lines have approximately the same strength. The "E" line is weak in infrared absorption measurements be-

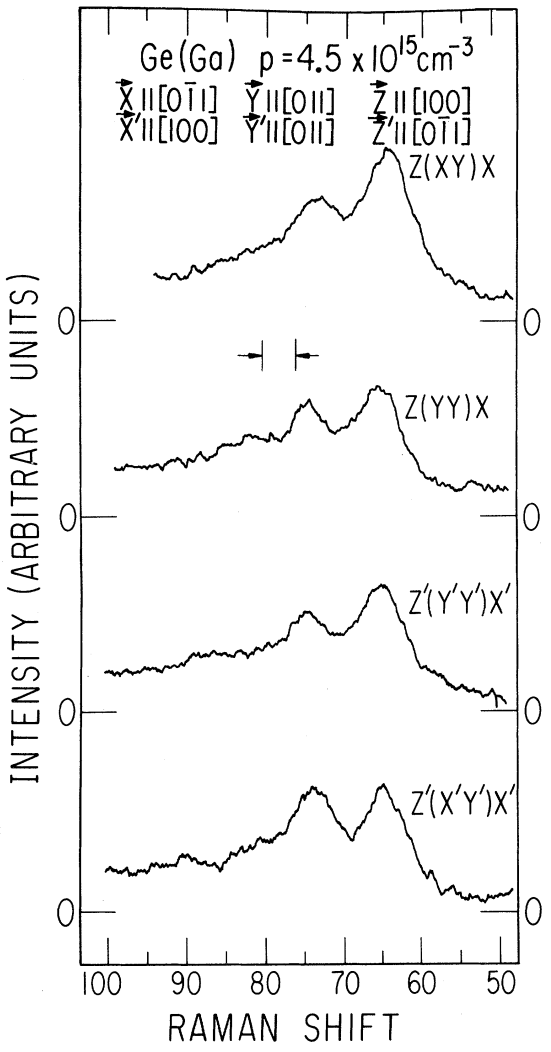

FIG. 2. Polarized Raman spectra of gallium acceptors in germanium.

cause it corresponds to an s-to-s transition, an electric dipole transition which is, in the first approximation, forbidden. An s-to-s Raman transition is, in contrast, highly favored. A transition lower in energy than the s-to-s transition was not observed. Such a transition constitutes a prominent feature of the acceptor spectra in silicon.[11] It has been suggested[11,15] that this low-energy transition may end on a state derived from the lower silicon valence band; there are no such states in germanium.

Mendelson and James[68] have calculated the wave functions of the acceptor states and have shown that the three states involved in the "E" and "C" transitions belong to the Γ_8 manifold. The two lines should therefore show identical Raman selection rules, which is verified, as shown in Fig. 2. A transition from a Γ_8 to a Γ_8 state can be observed if and only if the reduction of the direct product $\Gamma_8 \otimes \Gamma_8$ contains one or more of the irreducible representations according to which the polarizability tensor transforms. The direct product can be straightforwardly reduced with the aid of character tables[73]:

$$\Gamma_8 \otimes \Gamma_8 = \Gamma_1 + \Gamma_2 + \Gamma_3 + 2\Gamma_4 + 2\Gamma_5 , \tag{6}$$

where Γ_1, Γ_2, Γ_3, Γ_4, and Γ_5 are irreducible representations of the full double tetrahedral group. Of the species appearing in Eq. (6), Γ_1, Γ_2, and Γ_4 are Raman active.[56] Since the Γ_1, Γ_2, and Γ_4 species all have different polarization characteristics, it is expected that the observed Raman lines do not show a high degree of polarization.

Figure 3 shows the concentration dependence of the gallium acceptor spectrum. While the lines are well resolved at an impurity concentration of 4.5×10^{15} cm^{-3}, the lines are seriously broadened by wave-function overlap at $p = 2.5\times10^{16}$ cm^{-3}. At an impurity concentration of 7.5×10^{16} cm^{-3}, no structure is seen in the spectrum which at that

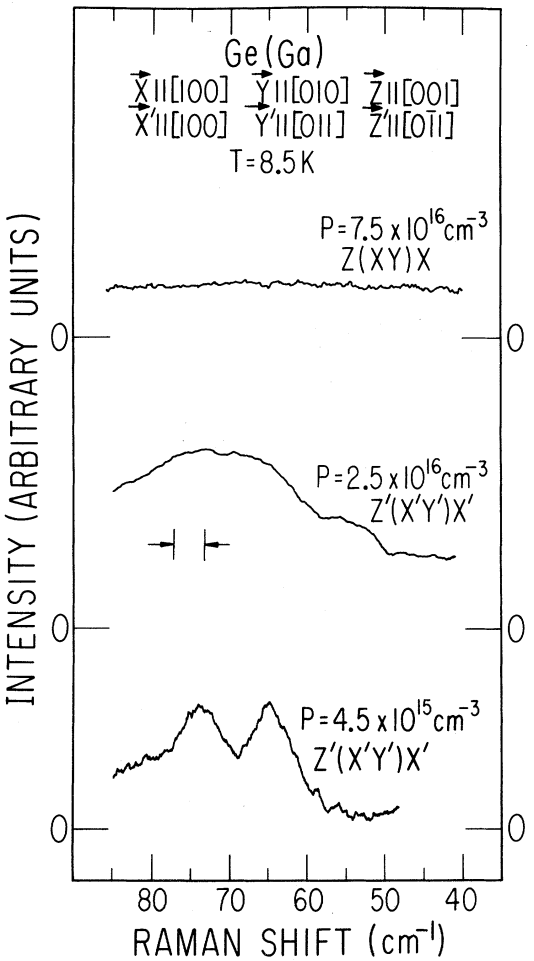

FIG. 3. Concentration dependence of the Raman spectrum of gallium-doped germanium.

concentration becomes a broad continuum. This broadening effect is striking considering the fact that the metal-nonmetal transition is known from conductivity measurements to occur at an impurity concentration near $p = 3\times10^{17}$ cm^{-3}. The broadening can be understood, however, when we consider the much more extended nature of the wave function associated with such high-lying hole states. The excited states therefore form a "band" at a lower impurity concentration than do the lower-lying states. The term "band" as it is applied here simply means a continuum of states; we cannot have a band structure in the single-crystal sense for the impurity ions since these ions occupy random sites, and do not exhibit translational symmetry. As the concentration increases, therefore, the energy required to excite a hole into a delocalized "band" decreases. This gradual delocalization might be responsible for the concentration dependence of the excitation energy ϵ_2 observed in conductivity experiments[36] (see also Sec. III D).

D. Semiconductor-to-metal transition

As the concentration of group-III or group-V impurities in a group-IV semiconductor such as germanium is increased to a critical concentration n_c, a semiconductor-to-metal transition, or Mott transition, takes place.[74] The Fermi level, normally located at the middle of the band gap in the pure material, is displaced by the presence of the nonisoelectronic impurities, but at an impurity concentration of n_c it has not moved sufficiently to penetrate either the valence or conduction band. Metallic conduction is then thought to take place in an "impurity band." Although a considerable amount of work, both experimental and theoretical, has been published on the metal-nonmetal transition,[75] there is very little knowledge about the role played by the discrete excited states of the impurity in such a transition. In particular, the characteristics of the "impurity band" are poorly understood.[76,77] The temperature dependence of the conductivity on n-type Ge measured by Fritzsche and Cuevas[78] can be fitted with a function of the form

$$\sigma(T) = \sum_{i=1}^{3} \sigma_i e^{-\epsilon_i/kT}, \tag{7}$$

with $\sigma_1 \gg \sigma_2 \gg \sigma_3$ and $\epsilon_1 > \epsilon_2 > \epsilon_3$. Here ϵ_1 is interpreted as being the energy required to eject a localized electron into the conduction band, while ϵ_2 and ϵ_3 are activation energies required to eject the electrons into a split "impurity band." ϵ_3 appears only if the material is compensated and is therefore the hopping energy. ϵ_2 is strongly concentration dependent and is interpreted as being the energy required to remove an electron from a donor site and place it on a donor already accommodating an electron, thereby forming a negatively charged donor (hence the name of ϵ_2 or D^- band). As the concentration is increased, ϵ_2 decreases and reaches zero at the critical concentration n_c. Mott's model[79] of the transition leads to the conclusion that no bound state of an electron around an impurity can exist when the screening length λ_s defined by

$$1/\lambda_s = 4m^*e^2n^{1/3}/\epsilon_0\hbar \tag{8}$$

becomes equal or smaller than the Bohr radius

$$a_H = \epsilon_0\hbar^2/m^*e^2 . \tag{9}$$

Solving for n yields a critical concentration given by

$$n_c^{-1/3} = 4a_H . \tag{10}$$

In this homogeneous model, each free electron contributes to the screening process and tends to lower the binding energy of all the other electrons, and a sharp transition in the dc conductivity[80] is therefore predicted. Cohen and Jortner,[81] on the other hand, suggest that the local density fluctuations, which are expected to occur in the impurity-site distribution, lead to an inhomogeneous mixture consisting, near the critical concentration, of submacroscopic metallic and semiconducting regions. On the metallic side of the transition, the metallic regions are sufficiently large that continuous paths extend throughout the crystal, while these metallic regions are unconnected on the semiconducting side of the transition. In this inhomogeneous model, the transition is predicted to be smooth, and both semiconducting regions and metallic regions are predicted to coexist near the critical concentration.

Figure 4 shows the spectrum of As-doped Ge as a function of impurity concentration. As the concentration increases [Figs. 4(a)–4(c)], the valley-orbit line grows in magnitude. At an impurity concentration of $n = 5.4\times10^{16}$ cm^{-3}, the electronic Raman line develops a tail on its low-energy side; at an impurity concentration of 1.7×10^{17} cm^{-3}, a tail also appears on the high-energy side of the Raman line [Fig. 4(f)]. At $n = 5.5\times10^{17}$ cm^{-3} [Fig. 4(j)], the Raman spectrum is a broad continuum which extends into the anti-Stokes side of the laser line; the existence of this continuum indicates that the electron wave functions extend over many donor sites. Indeed, Ge doped with 5.5×10^{17} cm^{-3} As impurities is metallic[37]; the semiconductor-to-metal transition occurs at about $n = 3\times10^{17}$ cm^{-3}. The samples yielding the spectra shown in Figs. 4(i) and 4(j) are therefore metallic. The full width of half-maximum[82] (FWHM) of the Raman line shown in Fig. 4 is plotted as a function of impurity concentration in Fig. 5; the error bars for the higher-concentration samples are large because the linewidth of the Raman line is ill defined for those

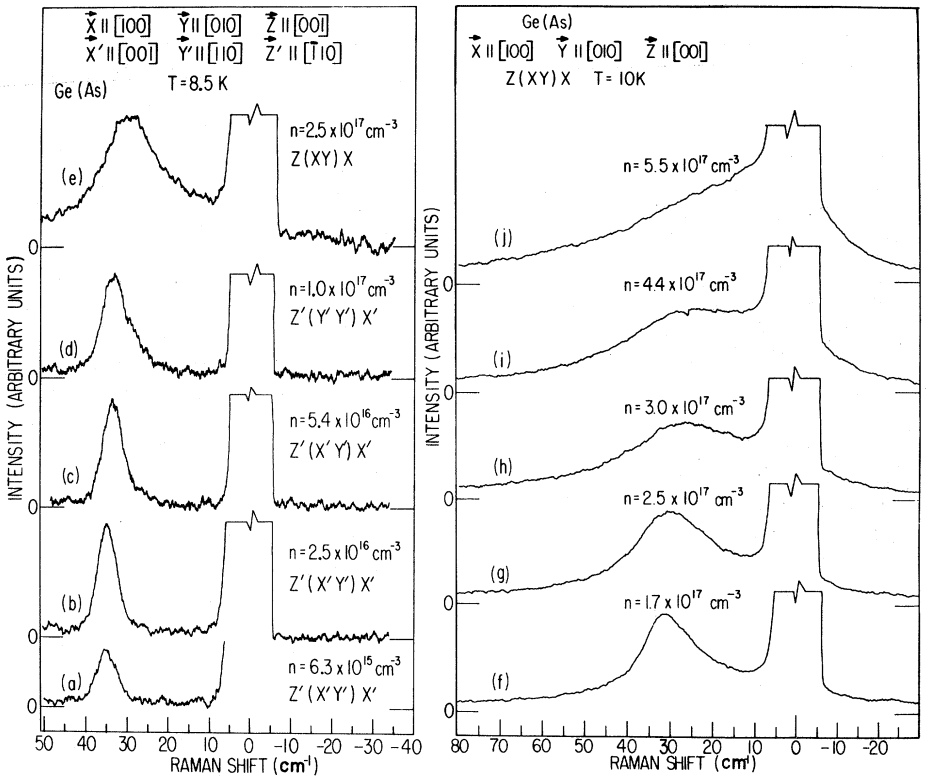

FIG. 4. Concentration dependence of the Raman spectrum of arsenic-doped germanium. The system gain for spectra (a) to (e) was approximately twice the gain for spectra (f) to (j).

samples since the spectrum has acquired a completely different shape. The linewidth shows a marked increase between $n = 2\times10^{17}$ and $n = 3\times10^{17}$ cm^{-3}. Also plotted in Fig. 5 is the resistivity of As-doped Ge as measured by Fritzsche[37]; the resistivity drops by nearly five orders of magnitude between $n = 2\times10^{17}$ and $n = 3\times10^{17}$ cm^{-3}, the concentration range over which the Mott transition takes place. The line shapes in Figs. 4(f) and 4(g) are particularly interesting because they suggest that the spectra consist of a broadened valley-orbit line superimposed upon a single-particle continuum. The resistivity of germanium doped with 1.7×10^{17} and 2.5×10^{17} cm^{-3} arsenic impurities confirms that the samples remain semiconducting at such concentration levels.[37] Also note that the peak of the valley-orbit line moves to lower wavenumber shifts as the impurity concentration is increased; this shift behavior is an indication of the presence of localized states above the critical concentration. If the spectra from the metallic samples were due only to metallic electrons, we would expect the peak in the spectra shown in Fig. 4 to move to higher-frequency shifts since the Fermi velocity increases with concentration (see Sec. III E).

In Ref. 7, the Raman line shapes were calculated by assuming an inhomogeneous model in which the overlap of the ground-state wave functions between two nearest arsenic neighbors is responsible for the broadening of the valley-orbit line. It was assumed that as the separation distance between two As impurities in germanium decreases, the two 1s ground states form a set of molecular bonding and antibonding states, split in energy, in analogy with the hydrogen molecule. This splitting depends upon the distance between the impurities and consequently upon the local impurity concentration. In this molecular model, the effect of local density

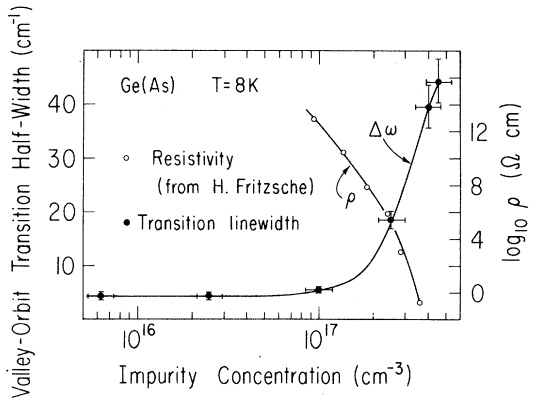

FIG. 5. Deconvolved linewidth of the valley-orbit Raman line of arsenic impurities in germanium as a function of concentration (left scale). Also shown (right scale) is the resistivity of Ge(As) as measured by Fritzsche (Ref. 33).

fluctuations is then to inhomogeneously broaden the $1s(A_1)$ ground state as well as the $1s(T_2)$ excited state, and consequently the valley-orbit line. The line shapes shown in Figs. 4(f)–4(i) were fitted in Ref. 7 by assuming that the impurities followed a Poisson site distribution.[83] Although this molecular model yields accurate fits and reasonable values for the parameters which enter in the fitting function, there are several difficulties associated with it. In particular, the assumption that the valley-orbit line shape is just given by the joint density of states implies that a transition starting on the ground state at one site and terminating on the excited state at any other site is allowed. This assumption is not valid because if the impurities do form molecular units, electronic transitions must be constrained to occur within such a unit. The line shape calculated when such a constraint is taken into account is much narrower and does not fit the observed Raman line shapes. The density fluctuations and molecular model as treated in Ref. 7 cannot quantitatively account for the observed broadening of the valley-orbit line.

We may nevertheless assume that the spectra shown in Figs. 4(f)–4(i) consist of a broadened valley-orbit line superimposed upon a single-particle background. It is a reasonable assumption since both the model of Mott and the model of Cohen and Jortner (CJ) predict that, near the critical concentration, the Raman lineshapes consist of two such contributions. In the CJ model, static density fluctuations lead to the coexistence of metallic and semiconducting regions; the semiconducting regions give rise to an inhomogeneously broadened valley-orbit line while the metallic regions are responsible for the single-particle background. According to Mott, temporal fluctuations in the number of momentarily singly occupied donors yield a lifetime broadened valley-orbit line, while doubly occupied donors are responsible for the single-particle background.

The single-particle background in Fig. 4(f)–(i) can be assumed to have the same shape as the spectrum shown in Fig. 4(j) because the single-particle excitation spectrum is not, except for its magnitude, very concentration dependent: the characteristic frequency determined by the Fermi velocity (see Sec. III E) is proportional to only $n^{1/3}$. Let $I_M(\omega)$ represent the spectrum shown in Fig. 4(j). The spectra shown in Figs. 4(f)–4(i) can then be written

$$I(\omega) = aI_M(\omega) + bI_{VO}(\omega) , \tag{11}$$

where $I_{VO}(\omega)$ is the valley-orbit contribution to the Raman intensity (strongly concentration dependent), and a and b are constants (also concentration dependent). With the assumption that the valley-orbit line is symmetrically broadened, the value of a is found uniquely when the function $I(\omega) - aI_M(\omega)$ is symmetric. The magnitude "a" of the single-particle background is a direct measure of the number of free electrons; that number is found to increase monotonically with concentration.

The value of the valley-orbit splitting is plotted as a function of impurity concentration in Fig. 6. The open triangles indicate values which have been obtained when the single-particle contribution to the line shapes shown in Fig. 4(f)–4(i) has been removed. The solid circles indicate values which have been obtained directly from Fig. 4(b)–4(d). It can be seen from Fig. 6 that, to within experimental error, no discontinuity appears at the critical concentration; also the data which were obtained by removing the background and the data which were obtained directly fall on the same straight line. This is the first observation of a dependence of the valley-orbit splitting upon the impurity concentration.

E. Raman scattering from free carriers

Single-particle excitations can be observed when electrons (holes) are free within the conduction (valence) band of the host crystal, or within an impurity band. In the limit of a large number of *noninteracting* electrons, each electron will scatter light independently, the frequency shift being given by the Doppler shift

$$\Delta\omega_i = \vec{q} \cdot \vec{V}_i , \tag{12}$$

where $\vec{q}$ is the momentum transfer and $\vec{V}_i$ the particle velocity. In this "single-particle" regime therefore, the Raman spectrum is a direct measure of the velocity distribution of the free elec-

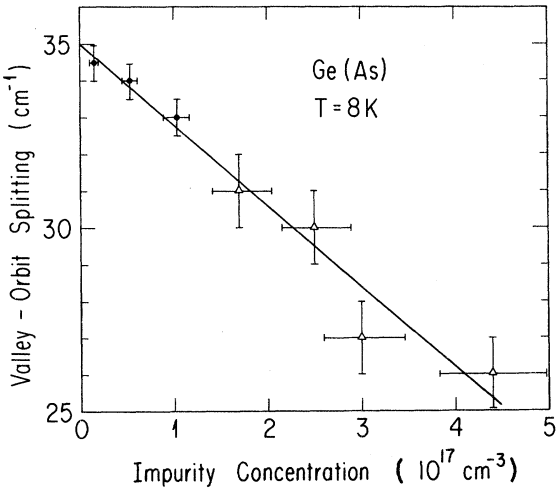

FIG. 6. Valley-orbit splitting as a function of impurity concentration obtained: (●) directly from spectra shown in Fig. 4(b)–(d); (△) by removing the single-particle background.

trons in the crystal. For example, in the case of a degenerate distribution, the cross section increases linearly with increasing wave-number shift up to qV_F, where V_F is the Fermi velocity, and shows a sharp cutoff at qV_F on the Stokes side of the laser line; there is no anti-Stokes scattering from a degenerate distribution at $T=0$ K. In the case of a classical plasma for which the average thermal velocity V_{th} is large compared to the Fermi velocity, the Raman line shape is Maxwellian, i.e., proporational to $\exp(-\omega^2/\omega_c^2)$ with a characteristic frequency shift given by $\omega_c = qV_{th}$. The Raman line shape is therefore, in the high-temperature limit, symmetrical about the laser line.

Figure 7 shows the temperature dependence of the single-particle spectra associated with Raman scattering from holes in Ge(Ga). The cutoff frequency for a concentration of $p = 7.5\times10^{16}$ cm^{-3} of light holes ($m^*/m = 0.04$) can be calculated to be 24 cm^{-1}. While the nonzero temperature, the instrumental and lifetime broadening[33] and the contribution from heavy holes smear the spectrum shown in Fig. 7 for $T = 8.7$ K, the spectrum is consistent with such a cutoff frequency. As the temperature increases, the anti-Stokes scattering becomes stronger and the spectrum becomes more symmetrical. In the high-temperature limit, the spectrum should resemble a Maxwellian distribution, with a frequency dependence proportional to $\exp(-\omega^2/\omega_c^2)$. We were unable to fit the high-temperature spectrum shown in Fig. 7 with the function $f(\omega) = A\exp(-\omega^2/\omega_c^2)$, where A and ω_c were treated as adjustable parameters. Instead, as shown in Fig. 8, the high-temperature spectrum can be very well fitted with a function of the form $f(\omega) = A\exp(-\omega/\omega_c)$, where A and ω_c were treated as adjustable parameters. The best-fitting value of ω_c was found to be $\omega_c = 28.1$ cm^{-1}. The reason why the spectrum cannot be fitted with $A\exp(-\omega^2/\omega_c^2)$ is understood: The high-temperature limit has not been reached at 92 K. At 92 K, the average thermal energy per hole is of the same order as the Fermi energy. The reason why the spectrum at 92 K follows an $\exp(-\omega/\omega_c)$ so well is not understood at this time. Platzman and Wolff[33] have derived a general expression for scattering from free carriers in a semiconductor. They consider the general Hamiltonian

$$H = \sum_i \frac{\vec{p}_i^{\,2}}{2m^*} + V(\vec{r}_1, \vec{r}_2, \ldots, \vec{r}_N) + \sum_i \frac{\hbar}{4m^{*2}c^2}(\vec{\nabla} V \times \vec{p}_i \cdot \vec{\sigma}_i), \quad (13)$$

where $V(\vec{r})$ is the effective periodic potential and where $\vec{\sigma}$ is the electron spin; the last term arises from the spin-orbit coupling. The scattering cross section calculated within the framework of a two-band model is given by

$$\frac{d\sigma}{d\Omega_1} = \frac{\omega_0}{2\pi\hbar c^2}\,\frac{\omega_1}{2\pi\hbar c^2}\,|M|^2, \quad (14)$$

where

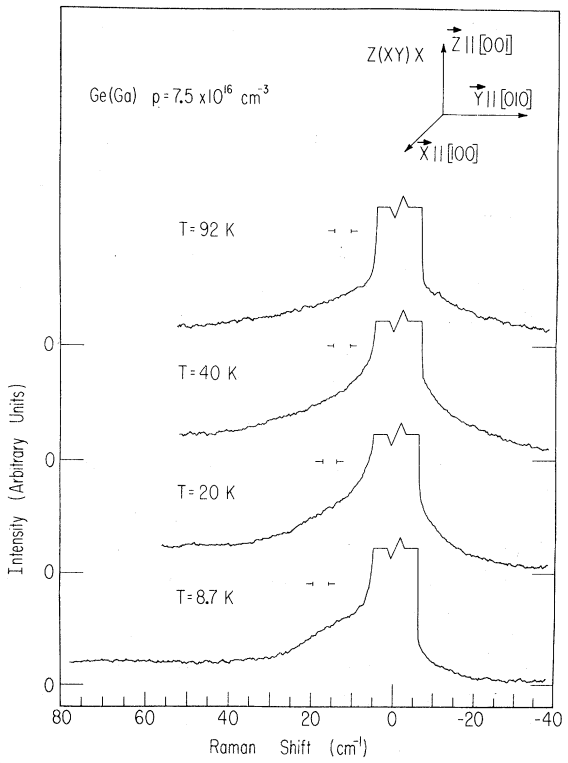

FIG. 7. Temperature dependence of the single-particle excitation spectrum of gallium-doped germanium.

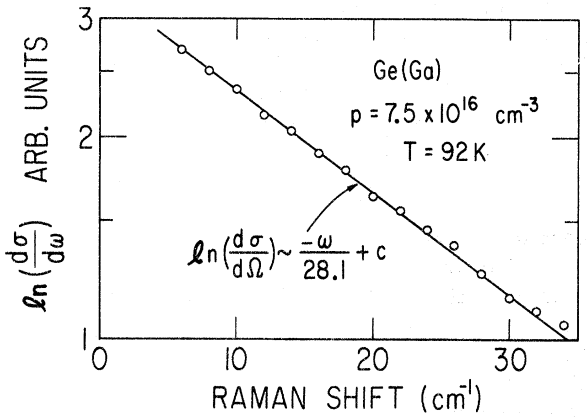

FIG. 8. Calculated fit (solid line) to the high-temperature single-particle excitation Raman line shape (○) shown in Fig. 7.

$$M \simeq \left(\frac{e}{c}\right)^2 \frac{2\pi\hbar c^2}{\omega_0\omega_1} \left\{ \frac{(\vec{\lambda}_0 \cdot \vec{\lambda}_1)}{m^*} \left[\left(\frac{E_G^2}{E_G^2 - (h\omega_0)^2} \right) \left(\frac{1}{m^*} - \frac{1}{m} \right) + \frac{1}{m} \right] + \left(1 - \frac{m_s}{m} \right) \left(\frac{\omega_0 E_G}{E_G^2 - (\hbar\omega_0)^2} \right) \frac{\vec{\sigma} \cdot (\vec{\lambda}_1 \times \vec{\lambda}_0)}{m_s} \right\} , \quad (15)$$

E_G is the band gap and m_s is the spin mass defined by

$$m_s = 2m/g , \quad (16)$$

g being the g factor of the electron. The familiar Thomson scattering matrix element can be derived from Eq. (15) by letting $\omega_0 \to 0$ and $g = 2$:

$$M = \left(\frac{e^2}{m^* c^2} \right) \left(\frac{2\pi\hbar c^2}{\omega_0 \omega_1} \right) (\vec{\lambda}_0 \cdot \vec{\lambda}_1) . \quad (17)$$

The first term in the sum of Eq. (15) is observed only in the parallel polarization configuration, while the second term appears only in the crossed polarization configuration. When a collection of interacting electrons is assumed, the first yields the cross section for charge-density fluctuations. The Raman cross section for an interacting electron gas is proportional to a structure factor[33] which contains a screening term. At high electron concentration, the charge-density fluctuations are screened and the first term in the sum of Eq. (15) is correspondingly small. The second term in Eq. (15) describes spin-density fluctuations which are not subject to screening. In high-concentration samples, therefore, the scattering from spin-density fluctuations is expected to be stronger than the scattering from charge-density fluctuations. It is to be noted that the light scattered from charge-density fluctuations or spin-density fluctuations is independent of the orientation of the crystal with respect to the laboratory axes. We note that the spectra shown in Fig. 7 were recorded in the crossed polarization configuration and are therefore due to spin-density fluctuations. The screening length for a plasma containing 7.5×10^{16} holes/cm^3 can be calculated to be less than 100 Å, which is much smaller than the wavelength of the exciting light. The long-wavelength charge-density fluctuations are therefore highly screened and do not contribute to the scattering of light. We further note that the impurity concentration is relatively close to the critical concentration for the Mott transition, at which the screening length is expected to be close to the Bohr radius.

The line shape shown in Fig. 4(j) is qualitatively similar to the single-particle spectrum shown in Fig. 7 ($T = 8.7$ K). Nearly all the scattering efficiency is on the Stokes side of the laser line. The cutoff frequency calculated from $\omega_c = qV_F$ lies between 7 and 127 cm^{-1}, the range reflecting the effective-mass anisotropy. The spectrum shown in Fig. 4(j) is consistent with such a range.

Figure 9 shows the temperature dependence of the single-particle spectrum shown in Fig. 4. As the temperature increases, the impurities ionize and the valley-orbit contribution to the Raman intensity decreases. The free electrons thus created contribute to the scattering of light from intervalley fluctuations, but a substantial fraction of the electrons scatter light into the anti-Stokes side of the laser line. At room temperature, all the impurities are ionized and we obtain a classical plasma. The Raman line shape at high temperature will not be a pure Maxwellian because of the high-mass anisotropy.

A light scattering process, which has not been

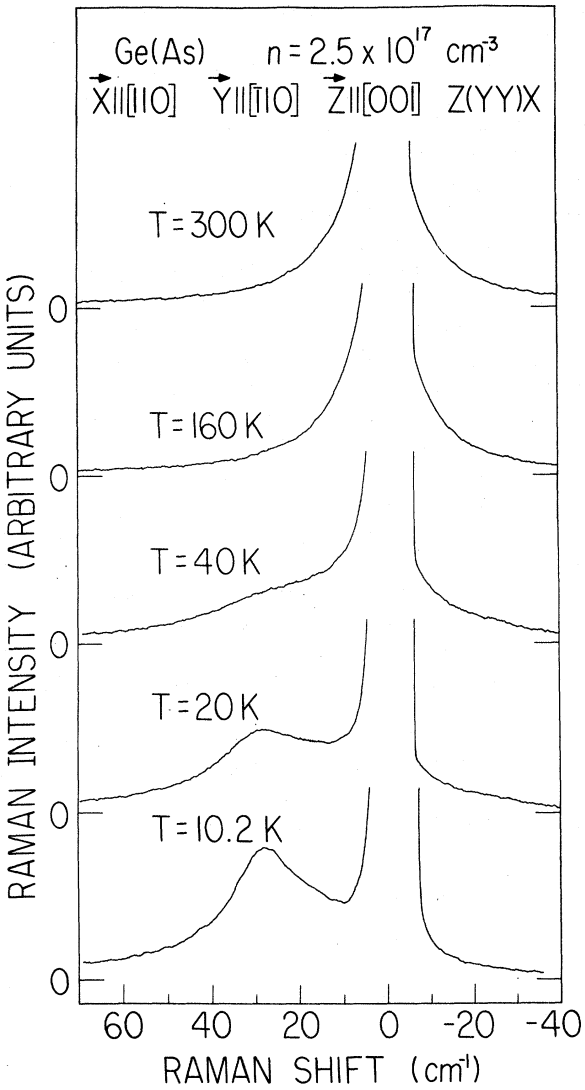

FIG. 9. Temperature dependence of the Raman spectrum of Ge(As).

observed previously, has been predicted by Platzman[84] to occur in multivalley semiconductors of which n-type Ge is an example. In the process considered by Platzman, the light will couple separately to the charge-density fluctuations in each valley, the total charge density remaining unchanged. The waves scattered from each valley then interfere, and the symmetry of the scattering cross section will reflect the symmetry of the crystal. This process is not subject to screening. Gantsevich *et al.*[85] have calculated the cross section for such a process:

$$\frac{d^2\sigma}{d\Omega_1\, d\omega_1} = \left(\frac{e^2}{c^2}\right)^2 \sum_{\alpha,\beta} \left(\vec{\lambda}_0 \cdot \frac{\vec{1}}{m_\alpha} \cdot \vec{\lambda}_1\right) \times \delta n_\alpha\, \delta n_\beta \left(\vec{\lambda}_0 \cdot \frac{\vec{1}}{m_\beta} \cdot \vec{\lambda}_1\right) . \qquad (18)$$

Here, $\vec{1}/m_\alpha$ is the inverse effective-mass tensor, and δn_α is the density fluctuation in the αth valley. It can be seen from Eqs. (18) and (15) that the Raman selection rules for the intervalley fluctuation mechanism will be identical to those of the valley-orbit transition.

Table I summarizes the Raman selection rules which have been derived for single-particle excitation in Sec. III. The valley-orbit Raman line has the same selection rules as the zone-center optic phonon in germanium, as does the Raman scattering from intervalley fluctuations; the charge-density fluctuations can be observed only in the parallel polarization configuration while the spin-density fluctuations can be observed only in the crossed polarization configuration. It can be seen from the table that the valley-orbit line can be separated from charge-density fluctuations in polarization configuration (a) and (b). Figure 10 shows the Raman spectra, taken in polarizations configurations (a) and (b), of the samples whose spectra are shown in Figs. 4(f), 4(h), and 4(j), respectively; the single-particle spectrum from the metallic sample, and the single-particle backgrounds from the other samples are present together with the valley-orbit line. The single-particle spectrum

TABLE I. Single-particle excitation selection rules.

Polarization configuration	$\vec{X} \parallel [100]$ $\vec{X}' \parallel [110]$ (a) $Z(XY)X$	$\vec{Y} \parallel [010]$ $\vec{Y}' \parallel [\bar{1}10]$ (b) $Z(YY)X$	$\vec{Z} \parallel [001]$ $\vec{Z}' \parallel [001]$ (c) $Z'(X'Y')X'$	(d) $Z'(Y'Y')X'$
Valley-orbit Raman line	yes	no	no	yes
Intervalley fluctuations	yes	no	no	yes
Spin-density fluctuations	yes	no	yes	no
Charge-density fluctuations	no	yes	no	yes

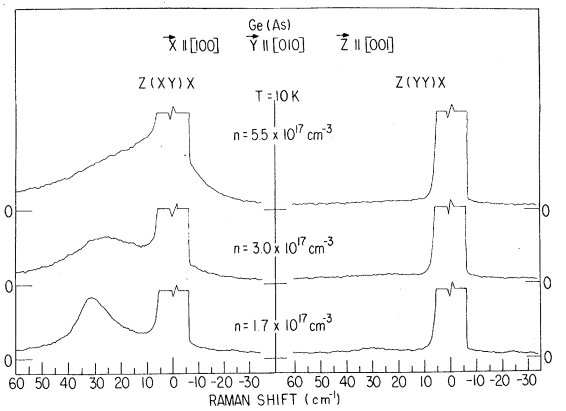

FIG. 10. Polarization dependence of the low-temperature Raman spectra of Ge(As); all spectra were recorded with the same system gain.

is therefore not due to charge-density fluctuations. Also charge-density fluctuations would be highly screened at these impurity concentration levels. The concentration is close to the critical concentration for the Mott transition for which the screening length is of the order of the donor Bohr radius, which is much smaller than the wavelength of the exciting light. Table I also shows that the valley-orbit Raman line can be separated from spin density fluctuations in polarization configurations (c) and (d). Figure 11 shows the Raman spectrum, in polarization configuration (c) and (d), of the sample whose spectrum is shown in Fig. 4(g). Again, the single-particle background appears only in the polarization configuration in which the valley-orbit line is Raman allowed. The single-particle background is therefore not due to spin-density fluctuations, which would appear only in polarization configuration (c). The single-particle background thus has the same polarization selection rules as the valley-orbit line and is due to intervalley

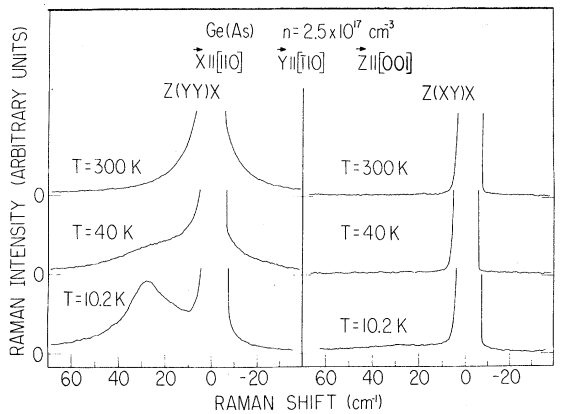

FIG. 11. Polarization dependence of the Raman spectra of Ge(As), at different temperatures; all spectra were recorded using the same system gain.

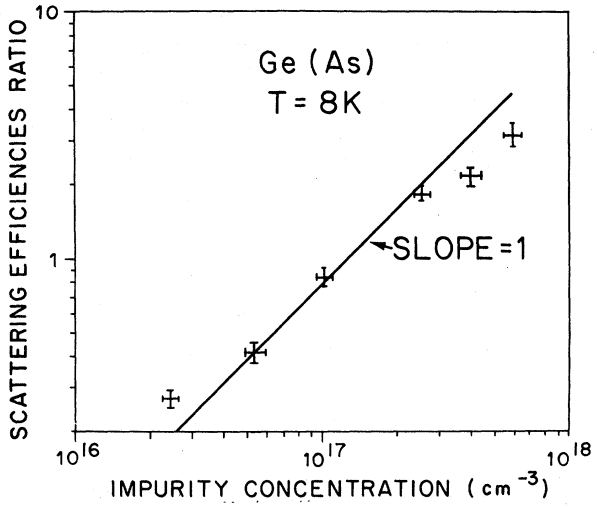

FIG. 12. Ratio of the electronic scattering efficiency to the scattering efficiency of the zone-center phonon in germanium plotted as a function of impurity concentration.

fluctuations.

The ratio of the integrated scattering intensity of the electronic line to the integrated scattering efficiency of the phonon is plotted as a function of concentration in Fig. 12. The electronic scattering efficiencies can be found by measuring the area under each curve in Fig. 4. The part of the line shape that is obscured by the laser line was estimated by joining a smooth line between the data on the Stokes side of the laser line and the data on the anti-Stokes side. The ratio is approximately proportional to the impurity concentration. The linear dependence of the integrated electronic cross section (Fig. 12) on concentration implies that the Raman cross section is the same whether the electron is bound or unbound. This result is further evidence that intervally fluctuations are responsible for the single-particle excitations [see Eq. (18)]. This seemingly striking result can be understood as follows. The wave function for the free electron is essentially a Bloch function. The wave function for the donor ground state is the product of a Bloch function and of a $1s$ envelope function [Eq. (4)]. When the $\vec{p}\cdot\vec{A}$ term (interband term) of the electron-photon interaction Hamiltonian is applied to the donor wave function, the effect of the momentum operator $\vec{p}$ on the $1s$ envelope function can be shown to be negligible[17] because its magnitude does not change significantly within one unit cell. The resulting matrix element is therefore not sensitive to the presence of the $1s$ envelope, i.e., the cross section is the same whether the electron is bound or unbound.

V. CONCLUSIONS AND SUMMARY

In conclusion, this work represents the first Raman scattering in the 2-μm spectral region. It also represents the first Raman study of the Mott transition. Electronic Raman processes can now be studied in materials which are opaque to commercially available 1.06-μm lasers but transparent at 2.1 μm. Very good agreement has been found between the theories described in Refs. 11, 16, 17, 58, 62, 65–68 on impurity states and the experiments performed on low-concentration samples of Ge(As). Group-theoretical predictions of the polarization characteristics of all the processes observed have been found to be obeyed within experimental error.

As the impurity concentration increases to a value larger than the critical concentration for the Mott transition, the valley-orbit line of Ge(As) broadens, a single-particle background appears and the spectrum changes continuously from one characteristic of a semiconductor to one characteristic of a metal. The valley-orbit splitting is found to decrease with increasing impurity concentration. The theory developed in Ref. 7 to fit the observed Raman line shapes has been found to be in error. Nevertheless it is possible that our Raman data coupled with a more sophisticated theoretical interpretation will help distinguish between the different models of the semiconductor-to-metal transition in Ge(As).

Light scattering from intervalley fluctuations was identified for the first time. Single-particle excitations from holes have also been observed. Further light-scattering experiments on germanium are now under way. A uniaxial-stress apparatus has been built[86] and has been used to shift the energy of the valley-orbit line. With stress applied along the [111] crystal axis the valley-orbit line splits into two components both of which move to higher energy; the single-particle background could thus be separated from the valley-orbit line in a stress experiment. Also, uniaxial stress in germanium has the property of shifting the energies of the conduction-band valleys and thereby effectively changing the number of valleys participating in the Mott transition.

Finally, the dependence of the Raman spectra upon the scattering angle (i.e., upon the wave vector transferred $\vec{q}$) should yield information upon the propagation regime[81] present in metallic samples.

ACKNOWLEDGMENTS

The author thanks Professor S. A. Solin for suggesting this work and for his enthusiastic support of this research project. His fairness and patience are sincerely appreciated. The author gratefully acknowledges the efforts of Professor P. J. Colwith whom he collaborated during the preliminary

phases of the research project described in this paper. The author wishes to thank Professor H. Fritzsche and Professor A. K. Ramdas for the donation of their samples and Professor M. H. Cohen for helpful discussions. Thanks are also due to Professor M. V. Klein for bringing to my attention the intervalley fluctuation mechanism and for giving me a copy of his manuscript prior to publication. Many helpful discussions with Dr. R. J. Kobliska, Dr. D. M. Hwang, M. Gorman, and R. J. Nemanich are acknowledged. The technical advice of R. J. Szara and H. Krebs will be remembered.

---

†Work supported by the AEC and in part by the NSF and the Louis Block Fund of the University of Chicago. Submitted in partial fulfillment of the requirements for the Ph.D. degree at The University of Chicago.

*Present address: Bell Laboratories, Holmdel, N. J. 07733.

[1]B. A. Weinstein and M. Cardona, Phys. Rev. B 7, 2545 (1973).

[2]R. K. Ray, R. L. Aggarwal, and B. Lax, in *Proceedings of the Second International Conference on Light Scattering in Solids*, edited by M. Balkanski (Flammarion, Paris, 1971), p. 288.

[3]F. Cerdeira and M. Cardona, Phys. Rev. B 5, 1440 (1972).

[4]J. H. Parker, Jr., D. W. Feldman, and M. Ashkin, Phys. Rev. 155, 712 (1967).

[5]G. G. McFarlane, T. P. McLean, J. E. Quarrington, and V. Roberts, Phys. Rev. 108, 1377 (1957).

[6]J. Doehler, P. J. Colwell, and S. A. Solin, Phys. Rev. B 9, 636 (1974).

[7]J. Doehler, P. J. Colwell, and S. A. Solin, Phys. Rev. Lett. 34, 584 (1975).

[8]R. J. Elliott and R. Loudon, Phys. Lett. 3, 189 (1963).

[9]J. T. Hougen and S. Singh, Phys. Rev. Lett. 10, 406 (1963).

[10]C. H. Henry, J. J. Hopfield and L. C. Luther, Phys. Rev. Lett. 17, 1178 (1966).

[11]G. B. Wright and A. Mooradian, Phys. Rev. Lett. 18, 608 (1967).

[12]G. B. Wright and A. Mooradian, Bull. Am. Phys. Soc. 13, 479 (1968).

[13]G. B. Wright and A. Mooradian, in *Proceedings of the Ninth International Conference on the Physics of Semiconductors, Moscow*, edited by S. M. Rykin and Yu U. Shmartsev (Nauka, Leningrad, 1968), p. 1067.

[14]J. M. Cherlow, R. L. Aggarwal, and B. Lax, Phys. Rev. B 7, 4547 (1973); B 9, 3633(E) (1974).

[15]D. D. Manchon, Jr. and P. J. Dean, in *Proceedings of the Tenth International Conference on the Physics of Semiconductors, Cambridge, Massachusetts*, edited by S. P. Keller, J. C. Hensel, and F. Stern (U.S. AEC Division of Technical Information Extension, Oak Ridge, Tenn., 1970), p. 760.

[16]P. J. Colwell and M. V. Klein, Phys. Rev. B 6, 498 (1972).

[17]P. J. Colwell, Ph.D. dissertation (University of Illinois, Urbana, 1971) (unpublished).

[18]P. J. Dean and R. L. Hartman, Phys. Rev. B 5, 4911 (1972).

[19]C. H. Henry and K. Nassau, Phys. Rev. B 2, 997 (1970).

[20]A. Mooradian and G. B. Wright, Phys. Rev. Lett. 16, 999 (1966).

[21]A. Mooradian, in *Advances in Solid State Physics*, edited by O. E. Madelung (Pergamon, New York, 1969), p. 73.

[22]A. Mooradian and G. B. Wright, in Ref. 13, p. 1020.

[23]J. F. Scott, T. C. Damen, J. Ruvalds, and A. Zawadowski, Phys. Rev. B 3, 1295 (1971).

[24]J. F. Scott, T. C. Damen, R. C. C. Leite, and J. Shah, Phys. Rev. B 1, 4330 (1970).

[25]F. A. Blum and A. Mooradian, in Ref. 15, p. 755.

[26]C. K. N. Patel and R. E. Slusher, Phys. Rev. 167, 413 (1968).

[27]D. T. Hon, S. P. S. Porto, W. G. Spitzer, and W. L. Faust, paper presented at Optical Society of America meeting, 1971 (unpublished).

[28]A. Mooradian, in *Light Scattering Spectra of Solids*, edited by G. B. Wright (Springer-Verlag, New York, 1969), p. 285.

[29]P. A. Wolff, Phys. Rev. 171, 436 (1968).

[30]A. Mooradian, Phys. Rev. Lett. 20, 1102 (1968).

[31]D. C. Hamilton and A. L. McWhorter, in Ref. 28, p. 309.

[32]A. Mooradian, in *Laser Handbook*, edited by F. T. Arecchi and E. O. Schulz-DuBois (North-Holland, Amsterdam, 1972), Vol. II, p. 1309.

[33]P. M. Platzman and P. A. Wolff, in *Waves and Interactions in Solid State Plasmas* (Academic, New York, 1973).

[34]G. Busch and H. Labhart, Helv. Phys. Acta 19, 463 (1946); 19, 167 (1946).

[35]C. Y. Yamanouchi, K. Mizugushi, and W. Sasaki, J. Phys. Soc. Jpn. 22, 859 (1967).

[36]H. Fritzsche, J. Phys. Chem. Solids 6, 69 (1958).

[37]H. Fritzsche, Phys. Rev. 125, 1552 (1962).

[38]W. Sasaki and R. de Bruyn Ouboter, Physica 27, 877 (1961).

[39]Y. Katayama and S. Tanaka, Phys. Rev. 153, 873 (1967).

[40]D. M. Finlayson and A. E. Mathewson, J. Phys. Chem. Solids 28, 1501 (1967).

[41]J. F. Woods and C. Y. Chen, Phys. Rev. 135, A1462 (1964).

[42]R. K. Sundfors and D. F. Holcomb, Phys. Rev. 136, A810 (1964).

[43]G. Feher, Phys. Rev. 114, 1219 (1959).

[44]S. Maekawa and N. Kinoshita, J. Phys. Soc. Jpn. 20, 1447 (1965).

[45]P. W. Anderson, Phys. Rev. 109, 1492 (1958).

[46]M. N. Alexander, Phys. Rev. 172, 331 (1968).

[47]J. I. Pankove and P. Aigrin, Phys. Rev. 126, 956 (1962).

[48]J. Doehler and S. A. Solin, Rev. Sci. Instrum. 43, 1189 (1972).

[49]Barber-Nichols Engineering Co., 6325 West 55th Street, Arvada, Col. 80002.

[50]Santa Barbara Research Center, 75 Coronar Drive, Goleta, Calif. 93017.

[51]Optical Coating Laboratory, Inc., 2789 Giffen Avenue, Santa Rosa, Calif.

[52]Jarrell-Ash Div., 590 Lincoln Street, Waltham, Mass. 02154.

[53]Karl Lambrecht Co., 4318 N. Lincoln Avenue, Chicago,

Ill. 60618.
[54]J. Doehler and S. A. Solin (unpublished).
[55]G. Placzek, in *Handbuch der Radiologie* (Academische Verlagsgesellschaft VI, Leipzig, 1934).
[56]R. Loudon, Adv. Phys. 13, 423 (1964); 14, 621(E) (1965).
[57]T. C. Damen, S. P. S. Porto, and B. Tell, Phys. Rev. 142, 570 (1966).
[58]W. Kohn, in *Solid State Physics*, edited by F. Seitz and D. Turnbull (Academic, New York, 1957), p. 257.
[59]J. C. Phillips, Phys. Rev. B 1, 1540 (1970).
[60]A. Baldereschi, Phys. Rev. B 1, 4673 (1970), and references therein.
[61]See, for example, C. Kittel, in *Quantum Theory of Solids* (Wiley, New York, 1963), Chap. 14.
[62]M. V. Klein (unpublished).
[63]J. H. Reuszer and P. Fisher, Phys. Rev. 135, A1125 (1964).
[64]V. V. Buzdin, A. I. Demeshina, Yu. A. Kurskii, and V. N. Murzin, Fiz. Tekh. Poluprovodn. 6, 2107 (1972) [Sov. Phys.-Semicond. 6, 1792 (1973)].
[65]J. M. Luttinger and W. Kohn, Phys. Rev. 97, 869 (1955).
[66]W. Kohn and D. Schecter, Phys. Rev. 99, 1903 (1955).
[67]D. Schecter, J. Phys. Chem. Solids 23, 237 (1962).
[68]K. S. Mendelson and H. M. James, J. Phys. Chem. Solids 25, 729 (1964).
[69]K. Suzuki, M. Okasaki, and H. Hasegawa, J. Phys. Soc. Jpn. 19, 930 (1964).
[70]K. S. Mendelson and D. R. Schultz, Phys. Status Solidi 31, 59 (1969).
[71]A. Baldereschi and N. O. Lipari, Phys. Rev. B 8, 2697 (1973).
[72]R. L. Jones and P. Fisher, J. Phys. Chem. Solids 26, 1125 (1965).
[73]H. Jones, in *The Theory of Brillouin Zones and Electronic States in Crystals* (North-Holland, Amsterdam, 1960).
[74]N. F. Mott, Proc. Phys. Soc. Lond. 62, 46 (1959).
[75]See, for example, Rev. Mod. Phys. 40, 1968.
[76]H. Nishimura, Phys. Rev. 138, A815 (1965).
[77]T. Lukes, B. Nix, and B. Suprapto, Philos. Mag. 26, 1239 (1972).
[78]H. Fritzsche and M. Cuevas, Phys. Rev. 119, 1238 (1960).
[79]N. F. Mott, Contemp. Phys. 14, 401 (1973).
[80]N. F. Mott, Phys. Rev. Lett. 31, 466 (1973).
[81]M. H. Cohen and Joshua Jortner, Phys. Rev. Lett. 30, 699 (1973).
[82]The deconvolved linewidth (FWHM) Γ_d was calculated from the observed linewidth Γ_{obs} and the observed laser linewidth Γ_L as follows: $\Gamma_d^2 = \Gamma_{obs}^2 - \Gamma_L^2$.
[83]N. Mikoshiba, Rev. Mod. Phys. 40, 833 (1968).
[84]P. M. Platzman, Phys. Rev. 139, A379 (1965).
[85]S. V. Gantsevich, V. L. Gurevich, V. D. Kagan and R. Katilius, in *Proceedings of the Second International Conference on Light Scattering in Solids*, edited by M. Balkanski (Flammarion, Paris, 1971), p. 94.
[86]M. Gorman, J. Doehler and S. A. Solin, Rev. Sci. Instrum. 45, 1592 (1974).